DEPARTMENT OF THE ARMY CORPS OF ENGINEERS

BEACH EROSION BOARD
OFFICE OF THE CHIEF OF ENGINEERS

THE DAMPING OF OSCILLATORY WAVES BY LAMINAR BOUNDARY LAYERS

TECHNICAL MEMORANDUM NO.117

THE DAMPING OF OSCILLATORY WAVES BY LAMINAR BOUNDARY LAYERS

TECHNICAL MEMORANDUM NO.117

BEACH EROSION BOARD
CORPS OF ENGINEERS

AUGUST 1959

FOREWORD

Any theoretical description of sediment movement under wave action depends on a thorough knowledge of kinematics of flow near the boundary, and the shearing forces exerted by this flow on the boundary, and on the sediment particles of the boundary. Experimental measurements of shearing stresses exerted on a smooth horizontal bottom due to the passage of oscillatory waves have been made, and this paper presents the results of these measurements. A theoretical approach is described, and coefficients are determined for laminar boundary layers from the experimental results.

The report was prepared at the Hydrodynamics Laboratory of the Massachusetts Institute of Technology in pursuance of contract DA-49-055-eng-16 with the Beach Erosion Board which provides in part for a study of the forces exerted by waves in moving sediment. This contract was under the general supervision of the Research Division of the Board. The author of the report, Peter S. Eagleson, is Assistant Professor of Hydraulic Engineering at M.I.T. The investigation was carried out under the administrative direction of Dr. Arthur T. Ippen, Professor of Hydraulics, and the direct technical supervision of the author. The experimental work and data analysis were performed by Mr. Francisco C. Go, Research Assistant.

Views and conclusions stated in this report do not necessarily represent those of the Beach Erosion Board.

This report is published under authority of Public Law 166, 79th Congress, approved July 31, 1945.

TABLE OF CONTENTS

LIST OF FIGURES AND TABLES

LIST OF NOTATIONS

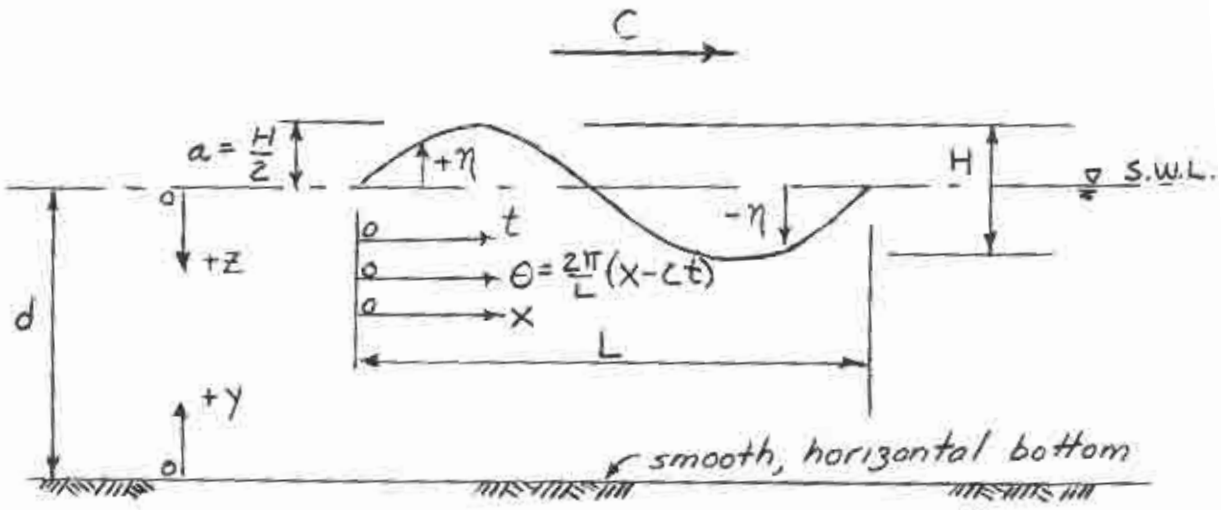

Definition Sketch

a = local wave amplitude, ft. or numerical constant

a_o = deep-water (undamped) wave amplitude, ft.

A = wave parameter

b = numerical constant

B = wave parameter

c = numerical constant

c_f = local resistance coefficient

C = wave celerity (phase velocity), ft./sec.

C_f = mean resistance coefficient

d = local stillwater depth, ft.

D = wave parameter

e = base of logarithms, 2.718 .....

E = local wave energy, ft.lb.

f = σU_{max}, ft./sec.^{2} or functional symbol

F = force, lb. or functional symbol

F_o = maximum value of forcing force, lb.

g = acceleration due to gravity, 32.2 ft./sec.^{2}

G = wave parameter

H = wave height, ft.

i = $\sqrt{-1}$

I = wave parameter

J = wave parameter

k = wave number, $2\pi/L$, ft.$^{-1}$

K = force amplification factor

ℓ = numerical constant

L = wave length, ft.

m = mass, slugs

n = viscous damping factor, lb.sec./ft., or ratio of group to phase velocities

p = pressure intensity, psf or spring constant, lb./ft.

$\mathcal{R}$, R = Reynolds number

s = numerical constant

t = time, sec. or plate thickness, ft.

T = wave period, sec., damped period of free vibration, sec.

T_o = natural period of free vibration, sec.

u = fluid particle velocity in x direction, ft./sec.

U = fluid particle velocity at $y = \delta$ in x direction, ft./sec.

v = fluid particle velocity in y direction, ft./sec.

x = horizontal coordinate direction origin as shown above for wave properties, otherwise arbitrary, ft.

y = vertical coordinate direction, origin at bottom, ft.

z = vertical coordinate direction, origin at still water surface ft.

α = phase angle, radians

β = $\left[\frac{\sigma}{2\nu}\right]^{1/2}$, sec.^{-1}

β_o = $\left[\frac{\sigma}{2\nu}\right]^{1/2}$, sec.^{-1}

γ = specific weight of fluid, lb./ft.^3

δ = boundary layer thickness, ft.

δ^* = displacement thickness, ft.

Δ = differential symbol

ϵ = wave damping factor

η = boundary layer parameter, y/δ or local height of free surface above the s.w.l., ft.

θ = wave phase angle, origin as shown above, radians

θ' = phase angle of boundary layer separation, radians

θ'' = phase angle of boundary layer separation, radians

Θ = momentum thickness, ft.

Λ = boundary layer velocity distribution parameter

μ = dynamic fluid viscosity, lb.sec./ft.^2

ν = kinematic fluid viscosity, $\text{ft.}^2/\text{sec.}$

π = 3.1415 .....

ρ = fluid mass density, slugs/ft.^3

σ = $\frac{2\pi}{T}$, sec.^{-1}

τ = shear stress, lb./ft.^2

τ_o = boundary shear stress, lb./ft.^2

ϕ = wave phase angle, radians

ψ = stream function, and phase lag, radians

THE DAMPING OF OSCILLATORY WAVES BY LAMINAR BOUNDARY LAYERS

By

Peter S. Eagleson
Massachusetts Institute of Technology

ABSTRACT

This report presents the results of an analytical and experimental investigation of the shearing stresses exerted on a smooth bottom by the passage of oscillatory water waves.

The experimental facilities consisted of a wave channel 90 feet long, 3 feet deep and 2½ feet wide. Test waves of various periods and heights were generated at one end of this tank by means of a horizontally reciprocating vertical bulkhead and were dissipated at the other end on a plane, smooth beach of 1:15 slope. All tests were conducted using a smooth bottom and a stillwater depth of 1.31 feet.

Force measurements were made by setting an isolated test panel in a false bottom placed in the wave channel and recording the time-history of instantaneous force on the panel during passage of the waves. Simultaneous measurements of instantaneous wave characteristics at the test panel were also obtained. The force measurements were corrected for pressure and inertia forces to obtain net tangential forces.

Average resistance coefficients and damping coefficients were derived in terms of the pertinent physical properties of the waves using existing small amplitude wave theory and assuming non-separating flow in a laminar boundary layer.

Analysis of the experimental results on the basis of these coefficients consistently showed the experimental bottom shearing stresses to greatly exceed those predicted by theory for the range of waves tested.

The boundary layer was then assumed to be disrupted each half wave cycle due to flow separation and the periodic regrowth of the layer was calculated by the approximate momentum technique. Resistance and damping coefficients calculated on this basis show, for the most part, excellent agreement with experiment.

I INTRODUCTION

A. Statement of the Problem

A thorough knowledge of the kinematics of flow near a boundary is a prerequisite to the quantitative understanding of fluid-induced motion of bottom sediments. The latter is a logical first step toward the prediction and control of erosion and deposition in channels, harbors and on beaches.

Recent efforts (1) aimed at a rational analytical description of the mechanics of the motion of discrete bottom sediments due to shallow-water waves have emphasized the need for experimental investigation of the properties of the bottom boundary layer under oscillatory water waves.

The measurement of one of these properties, bottom shearing stress, forms the basis of this report.

B. Scope of the Investigation

This study is restricted to the measurement of the shearing stresses exerted on a smooth, horizontal bottom due to the passage of oscillatory water waves of various characteristics.

II REVIEW OF PREVIOUS WORK

Interest in the effects of viscosity on oscillatory flows originated with considerations of water waves in the 17th century.

Stokes (2) pioneered in 1851 with the solution of the linearized dynamical equations in order to obtain the velocity distribution in non-separating laminar flow near a doubly infinite flat plate oscillating in its own plane. This solution has become known as the "shear wave".

Boussinesq (3) first formulated the theory of non-separating laminar boundary layers with respect to the motion of water waves by allowing for velocity and pressure variations parallel as well as normal to the solid boundary.

Keulegan (4) solved the Boussinesq problem for the case of small amplitude translational waves with an arbitrary free-stream velocity distribution restricted to negligible convective accelerations. He then calculated the gradual damping of solitary waves.

Basset (5) and Hough (6) solved the Boussinesq problem for small amplitude progressive oscillatory waves continuing the assumption of negligible convective accelerations.

Schlichting (7) has treated the shear wave problem of Stokes obtaining additionally the transient solution for the early stages of an oscillation commencing from rest.

Biesel (8) improved the accuracy of the Basset and Hough solutions for waves in very shallow water (i.e. d/L very small).

More recently Lhermitte (9) has described visual observations of the periodic regrowth of a separating laminar boundary layer under progressive oscillatory water waves. He presents the solution of the simplified dynamical (Navier-Stokes) equations for boundary layer thickness in terms of an undefined velocity distribution parameter. In a manner characteristic of most boundary layer calculations the thickness, δ, of the layer proves to be quite insensitive to the assumed velocity distribution while the bottom shearing stress is, by definition, critically dependent thereon.

In the early 1950's the science of supersonic aerodynamics stimulated an intense insterest in the effects of free-stream oscillations on laminar boundary layers. The primary problem giving rise to this interest was that of shifting separation points brought about by oscillating motion of a lifting vane and shock wave-boundary layer interactions.

Among the principal contributors were Lin (10), Nikerson (11) and Hill (12), who all considered laminar boundary layer growth on a semi-infinite flat plate due to a mean flow with superimposed minor periodic oscillations. Here approximate solutions of the dynamical equations in their non-linear form are given for special classes of flows separated by values of a frequency parameter, $x\omega/\overline{U}$, in which x is the distance from the leading edge of the plate, ω is the angular frequency of the oscillations and $\overline{U}$ is the average free stream velocity.

Lin (10) showed that for large values (greater than 10) of this frequency parameter the boundary layer solution was identical with Stokes' (2) shear wave irrespective of the relative magnitudes of mean and oscillatory velocities.

Nikerson (11) and Hill (12) have carried out solutions for small perturbations of a mean flow in the low and intermediate frequency ranges respectively.

Schuh (13) presents an approximate technique for the calculation of boundary layer growth in a field having an arbitrary temporal and spatial distribution of free stream velocity. The characteristic of this and other so-called "approximate" solutions to the non-linear dynamical equations is that the form of the velocity distribution must be assumed.

Ippen and Mitchell (17) studied the gradual damping of solitary waves and defined a boundary layer Reynolds Number which allows direct comparison of mean resistance coefficients for solitary waves with those for the conventional steady flow along a flat plate.

III THEORETICAL CONSIDERATIONS

A. Boundary Layer Thickness and Velocity Distribution

1. Non-Separating Flow

The case of two-dimensional, unsteady, laminar motion of an incompressible fluid in the x-y plane is described by the Navier-Stokes and continuity equations as follows:

$$\frac{\partial u}{\partial t} + u\frac{\partial u}{\partial x} + v\frac{\partial u}{\partial y} = -\frac{1}{\rho}\frac{\partial p}{\partial x} + \nu\left(\frac{\partial^2 u}{\partial x^2} + \frac{\partial^2 u}{\partial y^2}\right) \qquad [1]$$

$$\frac{\partial v}{\partial t} + u\frac{\partial v}{\partial x} + v\frac{\partial v}{\partial y} = -g - \frac{1}{\rho}\frac{\partial p}{\partial y} + \nu\left(\frac{\partial^2 v}{\partial x^2} + \frac{\partial^2 v}{\partial y^2}\right) \qquad [2]$$

$$\frac{\partial u}{\partial x} + \frac{\partial v}{\partial y} = 0 \qquad [3]$$

where gravity is the only body force.

Hough (6) neglected the non-linear convective acceleration terms in the above equations and defined a stream function,

$$\psi = \text{constant} - gy - p/\rho \qquad [4]$$

Assuming u, v and ψ are each proportional to $e^{i(kx - \sigma t)}$, his solution to Eqs. [1] through [4] yields:

$$\psi = (A\, e^{ky} + B\, e^{-ky})\, e^{i(kx - \sigma t)} \qquad [5]$$

$$u = [-\frac{1}{C}(A\, e^{ky} + B\, e^{-ky}) + (1+i)\,\beta/k\,(G\, e^{(1-i)\beta y} + D\, e^{-(1-i)\beta y})]e^{i(kx - \sigma t)} \qquad [6]$$

and

$$v = [\frac{i}{C}(A\, e^{ky} - B\, e^{-ky}) + G\, e^{(1-i)\beta y} + D\, e^{-(1-i)\beta y}]e^{i(kx - \sigma t)} \qquad [7]$$

In the above:

$$C = \text{wave celerity} = [(g/k)\tanh kd\,]^{1/2} \qquad [8]$$

$$k = \frac{2\pi}{L}, \quad \sigma = \frac{2\pi}{T}, \quad \beta = [\frac{\sigma}{2\nu}]^{1/2} \qquad [9]$$

Applying the following conditions for waves of very small amplitude:

a. $u = -\frac{\partial \psi}{\partial y}$, $v = \frac{\partial \psi}{\partial x}$

b. $u = o$, $v = o$ at $y = o$

c. $p_{yy} = -\gamma\eta$, $\tau = o$ at $y = d$,
where $p_{yy} = -p + 2\mu\frac{\partial v}{\partial y}$ and $\tau = p_{yx} = \mu(\frac{\partial v}{\partial x} + \frac{\partial u}{\partial y})$ [10]

d. $v = \frac{\partial \eta}{\partial t}$ at $y = d$ where $\eta = \frac{H}{2}e^{i(kx - \sigma t)}$

Hough found:

$$A = -\frac{CD}{2k}[(1+i)\beta - k] \qquad [11]$$

$$B = -\frac{CD}{2k}[(1+i)\beta + k] \qquad [12]$$

$$D = \frac{(1-i)k^2CH}{4\beta\sinh kd} = \frac{(1-i)k}{2\beta}\frac{f}{\sigma} \qquad [13]$$

$$G = \frac{(\frac{k}{\beta})^2[4+(\frac{k}{\beta})^2]}{C[4+(\frac{k}{\beta})^4]} e^{-(1-i)\beta d} (A e^{k\alpha} - B e^{-kd}) \quad [14]$$

Since β is of the order δ^{-1}, all terms involving G may be neglected.

Substituting Eqs. 11 through 13 and preserving only the real portions, Eqs. 6 and 7 become:

$$u = \frac{f}{\sigma}[\cos\Theta \cosh ky - e^{-\beta y}\cos(\Theta + \beta y) + \frac{k}{2\beta}\sinh ky (\sin\Theta - \cos\Theta)] \quad [15]$$

and

$$v = \frac{f}{\sigma}\left\{\sinh ky \sin\Theta - \frac{k}{2\beta}[\cosh ky (\sin\Theta + \cos\Theta) - e^{-\beta y}\cos(\Theta+\beta y) - e^{-\beta y}\sin(\Theta+\beta y)]\right\} \quad [16]$$

in which $\Theta = kx - \sigma t$

For small ky:

$$u = \frac{f}{\sigma}[\cos\Theta - e^{-\beta y}\cos(\Theta+\beta y) + \frac{k^2 y}{2\beta}(\sin\Theta - \cos\Theta)] \quad [17]$$

and

$$v = \frac{f}{\sigma}\left\{ky \sin\Theta - \frac{k}{2\beta}[\sin\Theta + \cos\Theta] + \frac{k}{2\beta}e^{-\beta y}[\cos(\Theta + \beta y) + \sin(\Theta + \beta y)]\right\} \quad [18]$$

For small k/β Eq. [17] may be reduced still further to:

$$u = \frac{f}{\sigma}[\sin\Theta - e^{-\beta y}\sin(\Theta - \beta y)] \quad [19]$$

wherein for convenience the origin of Θ has been moved $\pi/2$ radians toward the rear of the wave. Eq. [19] is identical with the "shear wave" solution of Stokes (2) for infinite wave length.

As is shown by Lamb (14), Eq. [19] represents the solution to the Navier-Stokes equations as written:

$$\frac{\partial u}{\partial t} = \nu\frac{\partial^2 u}{\partial y^2} + f\cos\Theta \quad [20]$$

under the conditions:

$$\begin{aligned} &a.\ u = o \quad \text{when } y = o \\ &b.\ u = f/\sigma \sin\Theta \text{ for large } \beta y \end{aligned} \quad [21]$$

The velocity distribution of Eq. [19] is plotted in Fig. [1-a] to a vertical scale measured in wave lengths of the shear wave. One wave length will be chosen as representing the boundary layer thickness, as given by shear wave theory:

$$\delta = 2\pi/\beta \quad [22]$$

2. Separating Flow

Examining Eq. [19] and Fig. [1-a] it can be seen that the velocity gradient at the wall becomes zero before the free stream velocity changes sign. This occurs at $\Theta = 3\pi/4,\ 7\pi/8$ according to Eq. [19] and indicates that in reality flow-separation will take place at or near these phase angles.

Due to this separation-induced disruption of the flow the boundary layer must, to some extent, reform each half wave cycle.

It will be assumed here that the reformation is complete yielding a boundary layer thickness which varies, twice each wave cycle, from zero to a maximum thickness the location of which is controlled by the position of the separation point. This assumption is shown for two different velocity distributions in Figs. [1-b] and [1-c].

The velocity distribution within this assumed laminar boundary layer will be first determined by the Karman-Polhausen technique. [See Schlichting (7) pg. 207].

If u is the instantaneous velocity, u(x, y, t) as before and U is the free stream velocity, U(x, t), then it is assumed that:

$$\frac{u}{U} = f\,(y/\delta) = f\,(\eta) = a\eta + b\eta^2 + c\eta^3 + d\eta^4 + s \quad \text{in the range } o \leq \eta \leq 1 \qquad [23]$$

It is further assumed that the vertical velocity, v, may be considered negligible which then eliminates vertical dynamic pressure gradients as well.

The following boundary conditions will be prescribed:

$$\left.\begin{array}{ll}
\text{a.} & u = o \quad \text{at } y = o \\
\text{b.} & u = U \quad \text{at } y = \delta \\
\text{c.} & \dfrac{\partial u}{\partial y} = o \quad \text{at } y = \delta \\
\text{d.} & \dfrac{\partial^2 u}{\partial y^2} = o \quad \text{at } y = \delta \\
\text{e.} & \nu \dfrac{\partial^2 u}{\partial y^2} = \dfrac{1}{\rho}\dfrac{\partial p}{\partial x} \quad \text{at } y = o \quad \text{(simplification of Eq. 1)}
\end{array}\right\} \qquad [24]$$

It should also be noted that when dealing with functions, F (x, t), which are harmonic in space and time the following identity holds between differential operators on these functions:

$$\frac{\partial F(x,t)}{\partial t} = -c\frac{\partial F(x,t)}{\partial x} \qquad [25]$$

In the absence of vertical pressure gradients Eq. [25] may be used to rewrite Eq. [24-e] as follows:

$$\nu \frac{\partial^2 u}{\partial y^2} = \frac{1}{\rho} \frac{\partial p}{\partial x} = -\frac{\partial U}{\partial x} [U-C] \qquad [26]$$

Evaluating the constants, Eq. [23] becomes:

$$\frac{u}{U} = 1 - (1-\eta)^3 (1+\eta) - \frac{\Lambda}{6} \eta (1-\eta)^3 \qquad [27]$$

in which

$$\Lambda = \frac{\delta^2}{\nu} \left[\frac{C}{U} - 1 \right] \frac{\partial U}{\partial x} \qquad [28]$$

The momentum equation of the boundary layer may be written:

$$\frac{\tau_o}{\rho U^2} = 2 \frac{\textcircled{\scriptsize\#}}{U} \frac{\partial U}{\partial x} + \frac{\partial \textcircled{\scriptsize\#}}{\partial x} + \frac{\delta^*}{U} \frac{\partial U}{\partial x} - \frac{C}{U^2} \frac{\partial}{\partial x} (U\delta^*) \qquad [29]$$

in which $\frac{\textcircled{\scriptsize\#}}{\delta} = \int_0^1 \frac{u}{U} \left(1 - \frac{u}{U}\right) d\eta = \frac{37}{315} + \frac{\Lambda}{945} - \frac{\Lambda^2}{9072}$

and $\frac{\delta^*}{\delta} = \int_0^1 \left(1 - \frac{u}{U}\right) d\eta = \frac{3}{10} + \frac{\Lambda}{120}$ [30]

In addition, since $\tau_o = \mu \frac{\partial u}{\partial y}$ at $y = o$,

$$\frac{\tau_o}{\rho U^2} = \frac{\nu}{\delta U} \left(2 - \frac{\Lambda}{6}\right) \qquad [31]$$

Substituting Eqs. [28], [30] and [31] in Eq. [29] and collecting terms:

$$\frac{\partial \delta}{\partial x} = \frac{\delta^{-1}(2\nu) - \delta \left(\frac{\partial U}{\partial x}\right) (.37 - .18 \frac{C}{U}) + \delta^3 (\cdots) + \cdots\cdots}{\delta^o (.12U - .3C) + \delta^2 \left(\frac{\partial U}{\partial x}\right) \left(\frac{C-U}{\nu}\right) (.0032 - .025 \frac{C}{U})} \qquad [32]$$

Letting

$$U = \frac{f}{G} \sin \Theta \qquad [33]$$

and neglecting all terms in Eq. [32] of order δ and higher:

$$\frac{\delta^2}{\nu T} = 1.06\ (\theta' - \theta) \qquad \theta' - \pi < \theta \leq \theta'$$

$$\frac{\delta^2}{\nu T} = 1.06\ (\theta' + \pi - \theta) \qquad \theta' < \theta \leq \theta' + \pi \qquad [34]$$

in which θ' and $\theta' + \pi$ are the phase angles of flow separation at the boundary.

From Eq. [31] separation may be seen to take place where $\Lambda = 12$ (i.e. $\tau_o = 0$). Since $\frac{C}{U} > 1$ Eq. [28] may thus be approximated by:

$$\Lambda = \frac{\delta^2}{\nu T}\ (2\pi \cot \theta) \qquad [35]$$

Simultaneous solution of Eqs. [34] and [35] at $\Lambda = 12$ locates the separation points at:

$$\theta = 1.07 \text{ and } (\pi + 1.07) \text{ radians} \qquad [36]$$

Using the above approximation for the parameter Λ, the velocity distribution of Eq. [27] is plotted in Fig. [1-b].

B. Bottom Shear Stress

The local bottom shear stress will be given by

$$\tau_o = \mu \left(\frac{\partial u}{\partial y}\right)_{y=o} \qquad [37]$$

1. Non-Separating Flow; Shear Wave Velocity Distribution

For the shear wave, Eqs. [19] and [37] yield:

$$\tau_o = \mu \beta \frac{f}{\sigma} [\sin\theta + \cos\theta] \qquad [38]$$

The average shear stress under an entire wave on the basis of Eq. [38] is:

$$\bar{\tau}_o = \frac{1}{\pi} \int_{-\pi/4}^{+\frac{3\pi}{4}} \tau_o d\theta = 0.9 \mu \beta \frac{f}{\sigma} \qquad [39]$$

2. Separating Flow; Karman-Polhausen Velocity Distribution

For the Karman-Pollhausen velocity distribution:

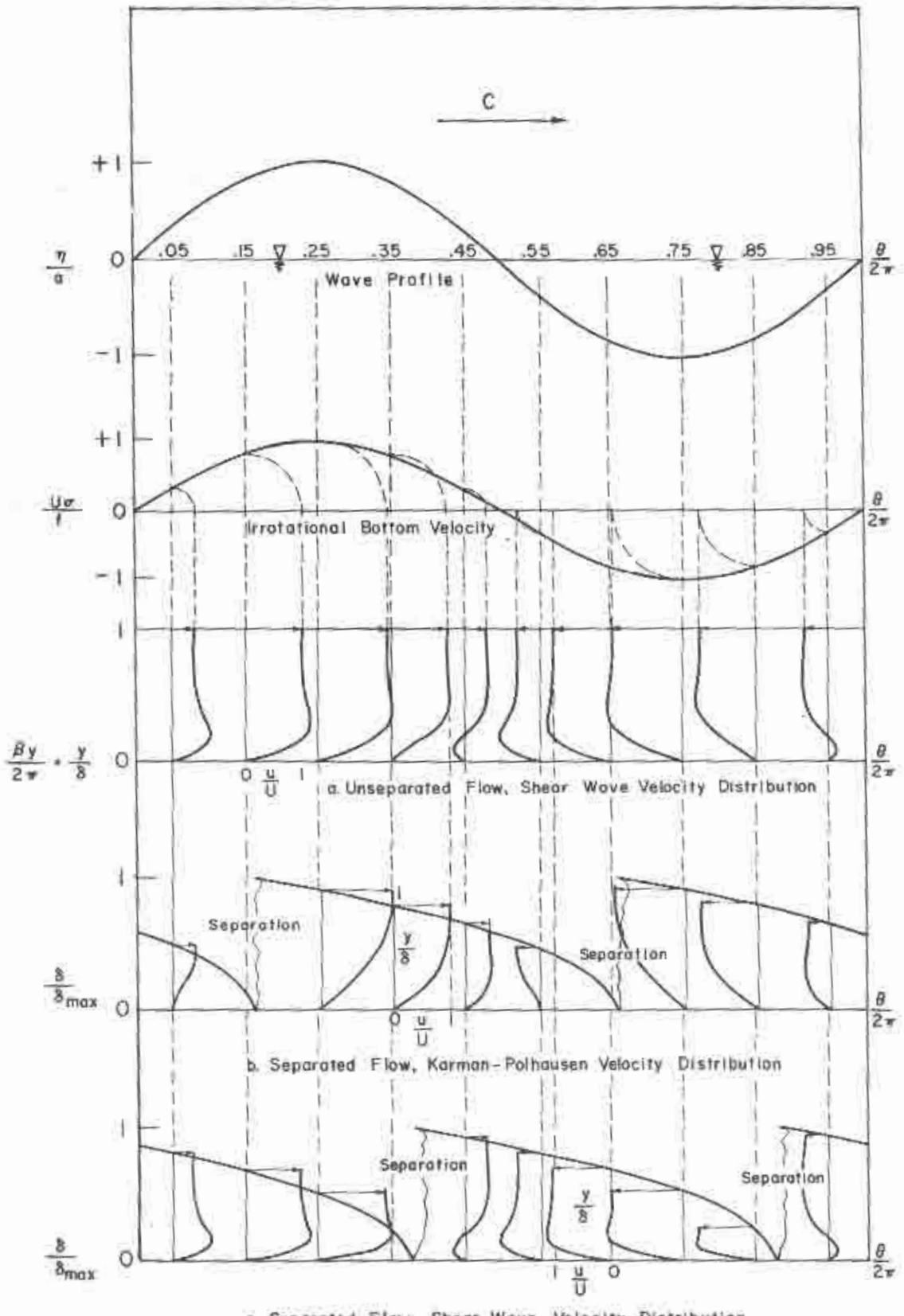

Fig. 1 Kinematics of the Boundary Layer

$$\tau_o = 0.29 \mu \beta_o \frac{f}{\sigma} [1.83\, \alpha^{-1/2} \cos\alpha - \alpha^{-1/2} \sin\alpha - \alpha^{1/2} \cos\alpha - 1.83\, \alpha^{1/2} \sin\alpha] \qquad [40]$$

$$\text{for} \quad \pi \geq \alpha > 0 \quad ; \qquad \alpha = 1.07 - \theta$$

in which

$$\beta_o = \left[\frac{\sigma}{2\nu}\right]^{1/2} \qquad [40\text{-}1]$$

and is independent of phase.

The average shear stress under an entire wave on the basis of Eq.[40] is:

$$\bar{\tau}_o = \frac{1}{\pi} \int_0^{\pi} \tau_o \, d\theta = 0.29 \mu \beta_o \frac{f}{\sigma} \qquad [41]$$

3. Separating Flow; Shear Wave Velocity Distribution

As Schlichting (7) points out, the thickness of the developing laminar boundary layer (on a flat plate in steady, uniform flow) as determined from a momentum analysis not only agrees well with that obtained from an "exact" solution of Eqs. [1] through [3] but also is quite <u>insensitive</u> to the form of the assumed velocity distribution.

Once boundary layer separation and regrowth are accepted the phase angle of the zone of most rapid boundary layer growth becomes critical with regard to the intensity of bottom shear stress produced. This phasing is determined by the separation points, the locations of which are extremely <u>sensitive</u> to the form of the velocity distribution.

Assuming that a velocity distribution obtained from a solution to the Navier-Stokes equations is more likely to be in accord with reality than the somewhat artificial Karman-Polhausen distribution, a combination of the two theories of paragraphs 1 and 2 above was obtained. A plot of the resulting near-bottom velocity distribution is shown in Fig. [1-c].

For this purpose Eq. [38] was modified by Eq. [22] to yield:

$$\tau_o = 2\pi \frac{\mu}{\delta} \frac{f}{\sigma} [\sin\theta + \cos\theta] \qquad [42]$$

With the separation points indicated by Eq. [42] (i.e. $\theta = \frac{3\pi}{4}, -\frac{\pi}{4}$) the boundary layer thickness as determined by a momentum analysis becomes:

$$\frac{\delta^2}{\nu T} = 1.06 \left(\frac{3\pi}{4} - \theta\right), \qquad -\frac{\pi}{4} \leq \theta < \frac{3\pi}{4} \qquad [43]$$

Combining Eqs. [42] and [43]:

$$\tau_o = 4.87 \mu \beta_o \frac{f}{\sigma} \phi^{-1/2} \sin\phi, \qquad \pi \geq \phi > 0 \qquad [44]$$

in which $\phi = \frac{3\pi}{4} - \theta$

The average shear stress under an entire wave on the basis of Eq. [44] is:

$$\bar{\tau}_o = 2.76 \mu \beta_o \, f/\sigma \qquad [45]$$

C. Resistance Coefficients

The conventional definitions of the steady-state local and average resistance coefficients are respectively:

$$c_f(x) = \frac{2\tau_o}{\rho U^2} \qquad [46]$$

and

$$C_f = \frac{2\bar{\tau}_o}{\rho \overline{U^2}} \qquad [47]$$

For the unsteady case of interest here we shall define these resistance coefficients and their associated Reynolds numbers as follows:

Locally -

$$c_f(\theta) = \frac{2\tau_o}{\frac{\rho}{\theta' - \theta}\int_{\theta}^{\theta'} U^2 \, d\theta} \qquad [48]$$

and, after Ippen and Mitchell (17),

$$R_\theta = \left| \frac{\int_{\theta}^{\theta'} U \, d\theta}{\nu} \right| = \left| \frac{\int_{\theta}^{\theta'} U^2 d\theta}{\nu} \right| \qquad [49]$$

Averaging over one-half wave cycle -

$$C_f = \frac{2\bar{\tau}_o}{\frac{\rho}{\pi}\int_{\theta'-\pi}^{\theta'} U^2 d\theta} = \frac{4\bar{\tau}_o}{\rho}\left(\frac{\sigma}{f}\right)^2 \qquad [50]$$

and

$$R = R_{\theta = \theta' - \pi} = \frac{\pi}{2}\frac{f^2}{\nu\sigma^3} \qquad [51]$$

in all of which θ' is the phase angle of the separation point under the wave crest.

Using these definitions we may derive the resistance coefficients for the three cases of interest:

1. Non-Separating Flow: Shear Wave Velocity Distribution

$$c_f(\theta) = \frac{8\nu\beta \frac{\sigma}{f} [\sin\theta + \cos\theta] (\pi - \theta)}{2(\pi - \theta) + \sin 2\theta}, \qquad 0 \leq \theta < \pi \qquad [52]$$

$$= \frac{f^2}{2\nu\sigma^3} [\pi - \theta + \frac{\sin 2\theta}{2}], \qquad [53]$$

and since $\theta' = 0$;

$$C_f = 3.6 \quad \nu\beta \frac{\sigma}{f} = 3.2 \, \mathbb{R}^{-1/2} \qquad [54]$$

2. Separating Flow: Karman-Polhausen Velocity Distribution

$$c_f(\alpha) = \frac{4.47 \nu\beta_o \frac{\sigma}{f} [1.83 \alpha^{1/2} \cos\alpha - \alpha^{1/2} \sin\alpha - \alpha^{3/2} \cos\alpha - 1.83 \alpha^{3/2} \sin\alpha]}{3.85 \alpha + 1.04 \cos 2\alpha + 1.61 \sin 2\alpha - 1} \qquad [55]$$

$$\mathbb{R}_\alpha = \frac{f^2}{2\nu\sigma^3} [\alpha + .42 \cos 2\alpha + .27 \sin 2\alpha] \qquad [56]$$

both for $\pi \geq \alpha > 0$ and $\alpha = 1.07 - \theta$

and since $\theta' = 1.07$ radians:

$$C_f = 1.16 \nu\beta_o \frac{\sigma}{f} = 1.03 \, \mathbb{R}^{-1/2} \qquad [57]$$

3. Separating Flow - Shear Wave Velocity Distribution

$$c_f(\phi) = \frac{39 \nu\beta_o \frac{\sigma}{f} \phi^{1/2} \sin\phi}{1 + 2\phi - \cos 2\phi} \qquad [58]$$

$$\mathbb{R}_\phi = \frac{f^2}{2\nu\sigma^3} [\phi + \tfrac{1}{2} - \tfrac{1}{2} \cos 2\phi] \qquad [59]$$

both for $\pi \geq \phi > 0$ and $\phi = 2.36 - \theta$

and since $\theta' = 2.36$ radians:

$$C_f = 11 \nu\beta_o \frac{\sigma}{f} = 9.75 \, \mathbb{R}^{-1/2} \qquad [60]$$

D. Damping Coefficients

For calculation of amplitude attenuation the effect of bottom resistance is conventionally contained in a damping coefficient or modulus of decay, ϵ, defined by

$$a = a_o e^{-\epsilon \frac{x}{L}} \qquad [61]$$

in which "a" is the variable wave amplitude and a_o its original, undamped value.

Considering, still, only viscous motions the decrease of wave energy results from the work involved in viscous deformation.

For the two-dimensional motion shown in Fig. 2 the work done in producing the indicated deformation in time dt is given by the product of the shearing force $\tau \Delta x$ and the displacement, $\partial u/\partial y \, dy \, dt$.

The local, instantaneous, unit time rate of deformation work per unit of crest width is then:

$$\Delta \frac{dE}{dt} = \int_0^d \tau \frac{\partial u}{\partial y} \, dy \, \Delta x \qquad [62]$$

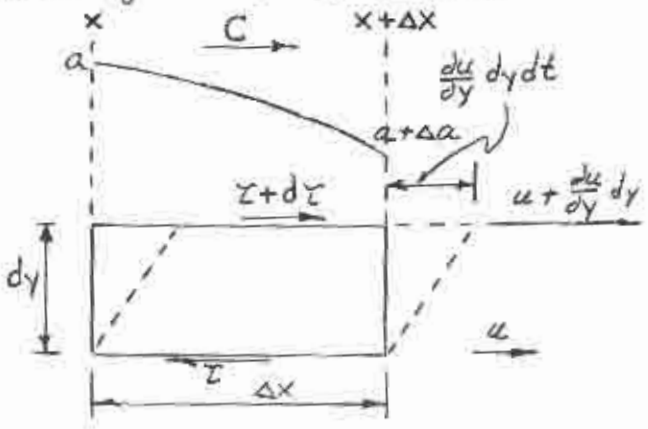

Fig. 2, Definition Sketch

The local, average, unit time rate at which work is done per unit of crest width by these viscous stresses becomes:

$$\Delta \overline{\frac{dE}{dt}} = \frac{1}{2\pi} \int_0^{2\pi} \int_0^d \tau \frac{\partial u}{\partial y} \, dy \, d\theta \, \Delta x \qquad [63]$$

From the standpoint of energy flux

$$\overline{\frac{dE}{dt}} = nEC \quad , \quad \text{ft. lb/sec/ft of crest width} \qquad [64]$$

in which n = ratio of group to phase velocities, i.e.

$$n = \frac{1}{2}\left[1 + \frac{2kd}{\sinh 2kd}\right] \qquad [65]$$

and, E = total wave energy per unit of surface area which may be written for waves of small steepness as:

$$E = \frac{\gamma H^2}{8} \approx \frac{\gamma a^2}{2} \qquad [66]$$

Considering the flux of energy through the control volume of Fig. 2 bounded by the bottom, water surface and two vertical stations x and x + Δx, Eq. [64] may be used to write:

$$\Delta \overline{\frac{dE}{dt}} = \left[\overline{\frac{dE}{dt}}\right]_x - \left[\overline{\frac{dE}{dt}}\right]_{x+\Delta x} = nc \frac{\gamma}{2} \left[a^2 - (a + \Delta a)^2\right] \qquad [67]$$

Equating Eqs. [63] and [67], taking the limit as $\Delta x \to 0$ and neglecting terms of order Δa^2;

$$\frac{da}{dx} = \frac{\int_0^{2\pi} \int_0^d \tau \frac{\partial u}{\partial y} \, dy \, d\theta}{2\pi \; nc \; \gamma \; a} \qquad [68]$$

Using Eq. [61] the damping coefficient then becomes:

$$\epsilon = \frac{\int_0^{2\pi} \int_0^d \tau \frac{\partial u}{\partial y} \, dy \, d\theta}{k \; n \; c \; \gamma \; a^2} \qquad [69]$$

For laminar velocity distributions of the form of Eq. [19] and for large βd, regardless of any time variation in β, Eq. [69] becomes:

$$\epsilon = \frac{\int_0^{2\pi} \left[\frac{\mu}{2} \beta \left(\frac{f}{\delta}\right)^2 + \tau_o U\right] d\theta}{2 \; k \; nc \; \gamma \; a^2} \qquad [70]$$

We may now use Eq. [70] to derive the decay moduli for the two cases of primary interest:

1. Non Separating Flow - Shear Wave Velocity Distribution,

$$\epsilon = \frac{\int_0^{2\pi} \tau_o U \, d\theta}{k \; nc \; \gamma \; a^2} \qquad [71]$$

or

$$\epsilon = \frac{4\pi^2}{\beta L \left(\sinh 2 \; kd + 2 \; kd\right)} \qquad [72]$$

2. Separating Flow - Shear Wave Velocity Distribution,

$$\epsilon = \frac{3.88\,\pi\,\mu\,\beta_o\left(\frac{f}{\delta}\right)^2 + \int_0^{2\pi} \tau_o U\, d\Theta}{2\,k\,n\,c\,\gamma\,a^2} \qquad [73]$$

or:

$$\epsilon = \frac{13.8\,\pi^2}{\beta_o L\,(\sinh 2\,kd + 2\,kd)} \qquad [74]$$

IV EXPERIMENTAL EQUIPMENT

All experiments were performed in the large wave channel in the Hydrodynamics Laboratory at the Massachusetts Institute of Technology.

Wave Generation and Measurement

The wave channel is 100 feet long, 2 1/2 feet wide and 3 feet deep (see Fig.[3-a]) and has glass walls over the entire 90 feet length of its working section. The bottom is horizontal and consists of 40 feet of smooth plate glass and 50 feet of smooth steel plate.

One end of the channel contains a smooth, plane impermeable beach of 1:15 slope which served to dissipate the wave energy.

Waves were generated at the other end by a horizontally reciprocating piston actuated by a hydraulic servomechanism with continuously variable speed and stroke. Fig. [3-b] shows an overall view of this generator.

Small disturbances found superimposed on the generated wave form were removed at the expense of a reduction in wave height by means of an expanded aluminum wave filter placed 10 feet downstream of the generator.

Measurement of wave characteristics was accomplished by means of two variable capacitance type wave profile wires spaced 10 feet apart near mid-channel.

A more detailed description of the above equipment may be found in Reference 17.

Force Measurement

At a test section, 46 feet from the wave generator, small, movable shear plates were set flush with a false bottom and suspended from above by means of a cylindrical pile. This pile support was protected from wave forces by an independently supported concentric cylindrical shield and extended through the free surface above which it was attached to a shear-sensitive force balance called a "portal gage". Fig. [4] shows a schematic view of this assembly.

Fig. 3a Wave Channel

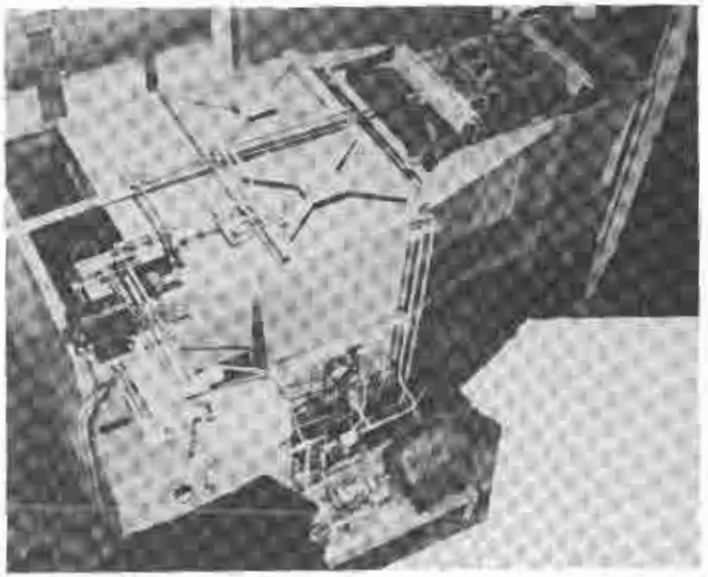

Fig. 3b Overall View of Wave Generator

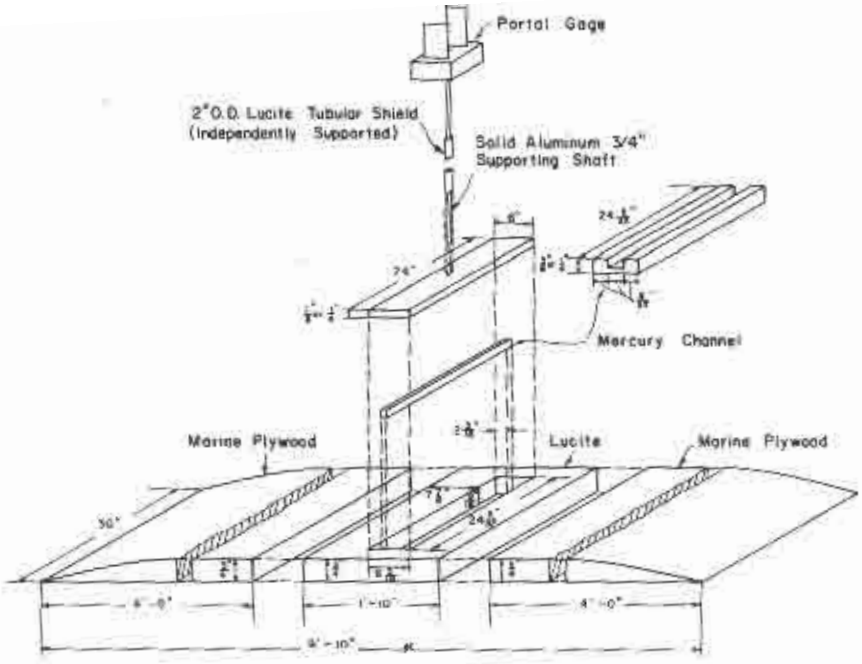

Fig. 4, "Exploded View" of Shear Plate Assembly

1. Shear plates - The test plates used were 2 feet wide (transverse to wave), 6 inches long (in direction of wave propagation), either 1/8" or 1/4" thick and were constructed of aluminum. They were supported from above by a 3/4 inch diameter aluminum rod 41 inches long. This rod was shielded by an independently supported concentric lucite tube of 1 1/4 inch I.D.

2. False bottom - A false bottom consisting of a piece of 3/4 inch marine plywood 8 feet long and 30 inches wide was placed in contact with the channel bottom at the test section. The plywood was tapered to a feather edge along its two short sides and was fixed to the channel bottom by screws into the transverse brass strips separating the glass bottom panels and by thin vertical braces extending through the free surface along the channel walls.

The board was divided into two pieces each 4 feet long by the insertion of a 3/4" lucite panel, 22 inches long. This panel was relieved, by milling, to receive the test plates. As shown in Fig. [4] this recess was machined larger than the test plates to allow a gap of 1/64" for motion of the plate.

A small raised channel running from wall to wall of the recess in a transverse direction was machined as the recess was constructed. To prevent flow through the clearance gaps and under the plate this channel was filled with mercury until the meniscus touched the underside of the plate. This seal was installed after the test plate was in position by injecting the mercury through a fine hole in the plate.

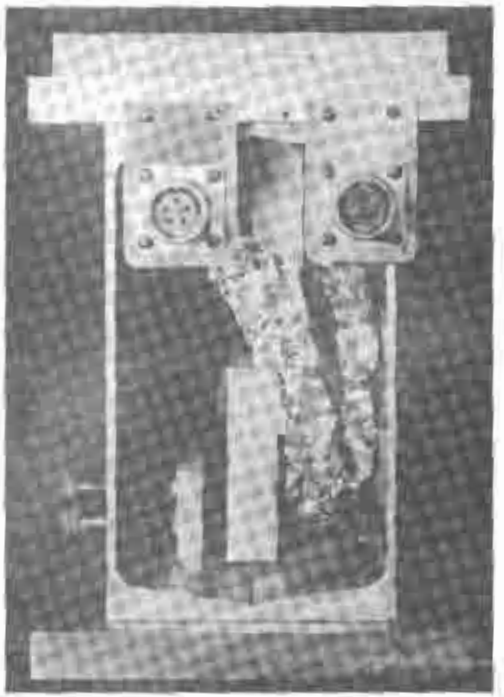

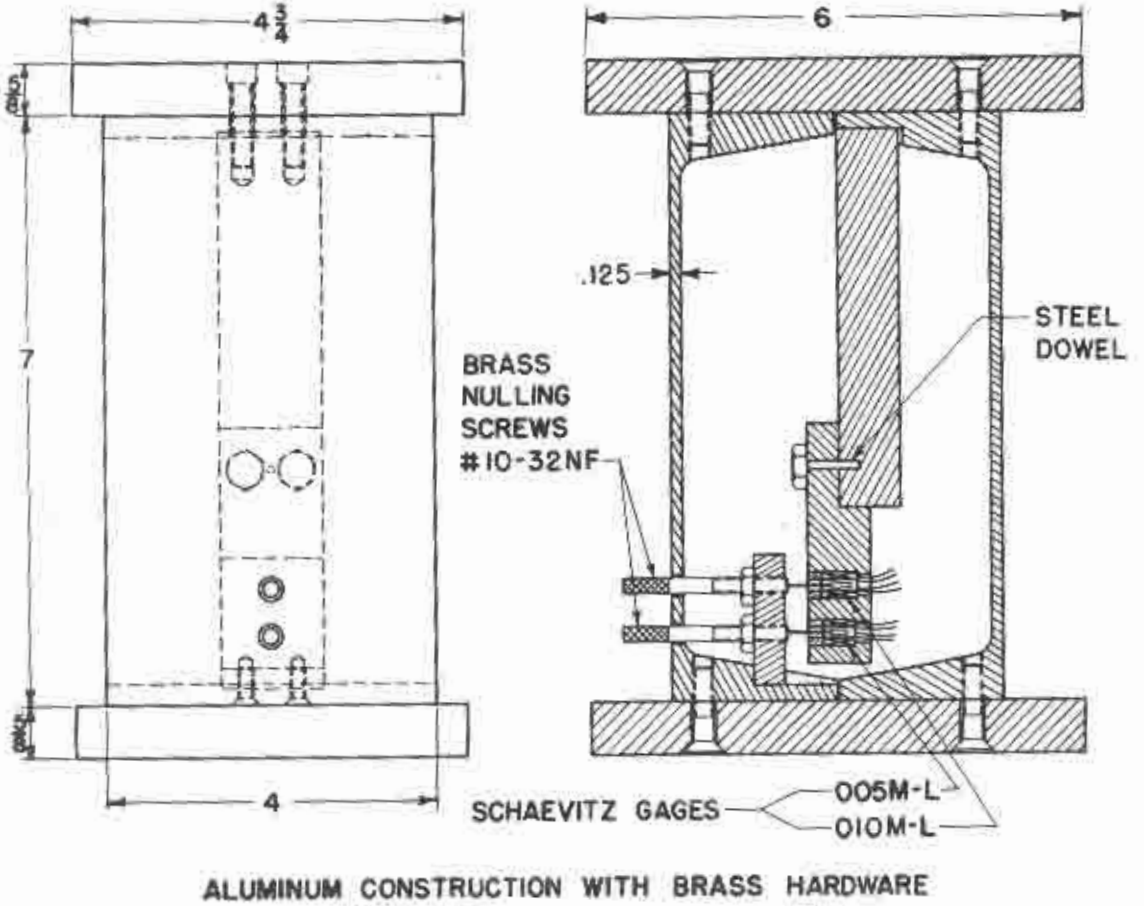

Fig. 5 Portal Gage, Photo and Schematic Diagram

The same longitudinal pressure gradient tending to cause through flow under the plate creates a differential pressure force on the transverse plate edges. As will be described in the next section this force is eliminated through use of two plates of different thickness. This requires, for the thinner plate, a higher mercury channel which was installed as shown in Fig. [4].

3. Force balance - (see Fig. [5]) The force gage was rigidly mounted above the wave channel and consisted of a portal type unit sensitive only to horizontal forces. The transducer of the gage was a linear differential transformer which measured the horizontal deflection of the bottom plate of the gage, that deflection being directly proportional to the force applied. The gage was statically calibrated by attaching a string to the rod supporting the test plate and extending this string horizontally over a pulley and down to a free-hanging weight pan.

4. Recording apparatus - A model 150 Sanborn recording oscillograph was used to register simultaneously, total force on the test plate and wave profile at and 10 feet "upstream" of the test plate centerline.

V EXPERIMENTAL PROCEDURES

A. Data Procurement

The 1/8" thick shear plate was mounted on its supporting pile and carefully adjusted to be flush with the false bottom and centered in its recess. During this process the wave channel contained about 1 or 2 inches of water.

The mercury seal was then filled by injection through the test plate and the cylindrical shield was adjusted for concentricity with the supporting pile.

The wave tank was then filled to 1.312 feet and both the wave gage and shear gages were calibrated. Descriptions of calibration techniques and sample calibration curves for these gages may be found in Ref. 16.

One of the 9 test waves was then established in the wave channel. Characteristics of these test waves are given in Table I.

After waiting several minutes for steady state conditions to be established a simultaneous record was taken of total force on the shear plate and of wave profile at the two gaging stations. This record was at least 6 wave lengths in length. A sample record is shown in Fig. [6].

This procedure was repeated for each of the test waves.

The 1/4" thick shear plate was then installed, calibrations were repeated and by very careful adjustment of the wave generator the same 9 test waves were established successively. Force records were again obtained for each test wave.

TABLE I Characteristics of Test Waves

Wave No.	Period (sec.)	Height (ft)	Length (ft)	Stillwater Depth (ft)
1	1.29	0.298	7.37	1.312
2	1.62	0.258	9.00	1.312
3	1.98	0.305	13.05	1.312
4	2.76	0.303	17.20	1.312
5	1.15	0.262	6.14	1.312
6	0.98	0.212	4.60	1.312
7	0.86	0.194	3.70	1.312
8	0.84	0.168	3.56	1.312
9	1.08	0.183	5.49	1.312

As a supplemental investigation records were taken of the damped and "undamped" free vibrations of the plate-rod-force balance system. To accomplish this the plate was displaced to the edge of the recess and released. For the damped case conditions duplicated those of the shear determinations. For the"undamped" case only air was in contact with the system. These determinations were repeated several times and averaged for calculating purposes. Sample records of the damped and "undamped" vibrations are shown in Fig. [7].

B. Data Analysis

1. Total Force Determination

From the record of wave profile taken at the shear plate the wave period was determined and 4 successive waves were each divided into 16 equal parts. These discrete phase angles were then located on the total force trace by projecting across the record at 90° to the time axis.

The total forces were picked off and values for the four waves averaged every $\pi/8$ radians.

The above process was carried out for both thicknesses of plate under each wave.

2. Correction for Inertial Force

In order to maintain a high natural frequency for the force balance-shear plate assembly, every attempt was made to limit its mass. The mass of

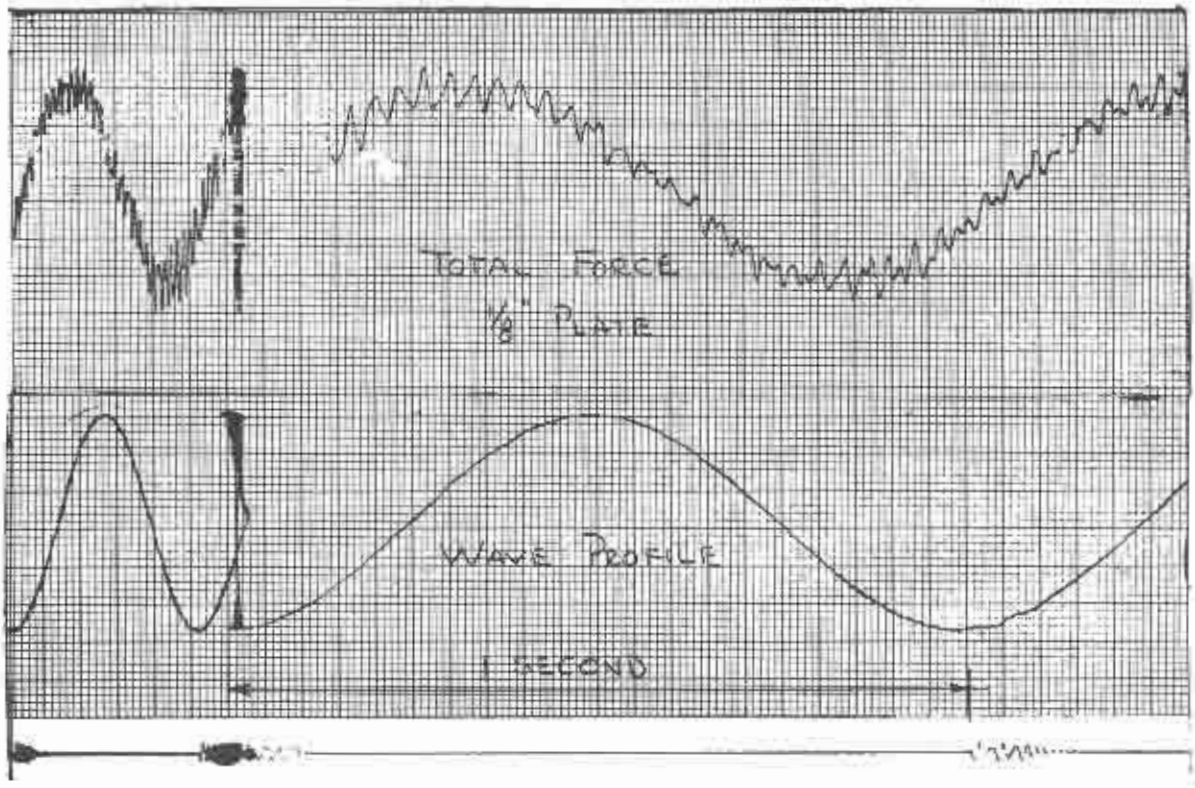

Fig. 6 Sample Force and Wave Profile Trace

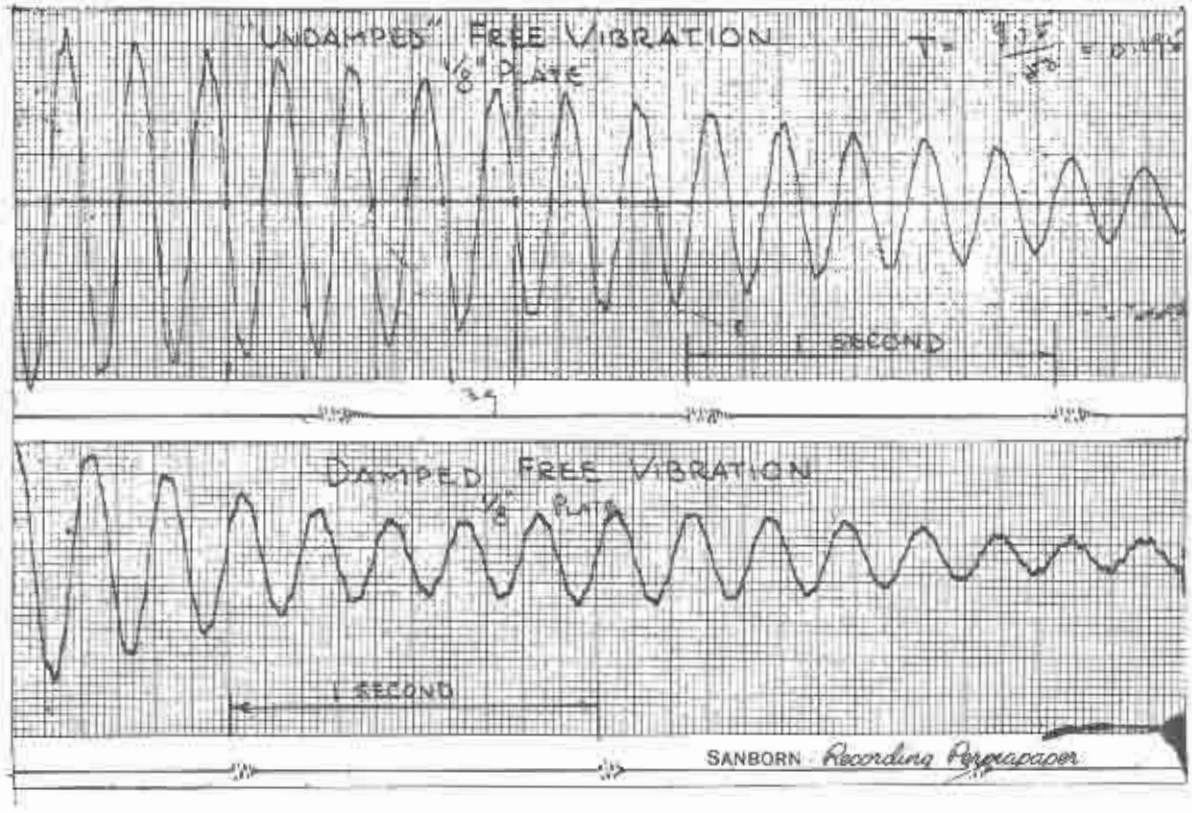

Fig. 7 Sample Damped and Undamped Free Vibrations of Shear Plate Assembly

the supporting rod was limited by using a small diameter and a light material. The attendant loss in stiffness acts contrary to mass reduction however by tending to lower the natural frequency.

A check of the plate accelerations actually experienced in the dynamic measurements indicated the advisability of correcting the measured total force for the effects of inertia.

The measuring system consists of two main units connected in series, the "portal" shear gage (Fig. [5]) and the supporting rod with attached shear plate. The spring constant of the dual-cantilever shear gage is about 1000 lb/in. (see Ref. 16), while that of the cantilevered supporting rod is about 6 lb/in.

Because of the great stiffness of the portal gage relative to that of the rod-plate assembly, the system was considered to have a single degree of freedom, i.e. that of the supporting rod in flexure as a cantilever.

The equation of motion for the vibrating plate can thus be written:

$$m\ddot{x} + n\dot{x} + px = F_o \cos \sigma t \qquad [75]$$

in which

m = actual and apparent mass of immersed plate and rod

n = viscous damping factor

p = spring constant

$F_o \cos \sigma t$ = assumed approximate form of forcing function (shear + pressure forces)

Solution of Eq. [75] for large t is given by Den Hartog (18) as:

$$px = \frac{p F_o \cos \sigma t}{\left[(p - m\sigma^2)^2 + n^2\sigma^2\right]^{1/2}} \qquad [76]$$

and $$\tan \psi = \frac{n\sigma}{p - m\sigma^2} \qquad [77]$$

where px is the actual signal from the force balance (heretofore called "total force") and ψ is the phase angle by which the total force lags the forcing function, $F_o \cos \sigma t$.

The "undamped"natural period, T_o (period of free vibration in air) and the damped natural period, T, (period of free vibration in water) were measured as described above and the spring constant was calculated from the structural properties of the system. The mass, m, and damping factor, n, were then calculated using their definitions as given by Den Hartog (18):

$$T_o = 2\pi \left[\frac{m}{p}\right]^{1/2} \qquad [78]$$

and

$$T = 2\pi \left[\left(\frac{p}{m}\right) - \left(\frac{n}{2m}\right)^2\right]^{-1/2} \qquad [79]$$

On the basis of Eq. [76] a correction factor, K, was calculated by which to multiply the measured total forces, i.e.

$$F_o \cos\sigma t = K\, px \qquad [80]$$

A summary of the measured properties and calculated correction factors is given in Table II.

The discrete average values of total force for each plate and wave were multiplied by the appropriate correction factor, K, listed in Table II and the modified values were shifted in phase by the appropriate angle, Ψ. A smooth curve was drawn through the resulting points.

3. Correction for Pressure Force

Because of local variations from the potential flow bottom pressure distribution due to (1) boundary layer growth, (2) dynamic pressures resulting from plate motion and, (3) momentary exposure of plate edges to stagnation pressures, it was felt advisable to measure the pressure forces rather than calculate them from potential theory.

The inertially corrected force values for the 1/8" plate were subtracted from those for the 1/4" plate for the same wave at common phase angles $\pi/8$ radians apart. The remainders were due to the net pressure force exerted on the thin faces of the plate which are normal to the direction of wave propagation.

It was assumed that the magnitude of this pressure force is directly proportional to the plate thickness, consequently the remainders of the above subtraction were, in turn, subtracted from the corresponding values of total force on the thin plate as corrected for inertial effects to yield the time-history of shear force.

As was shown by Ippen and Mitchell (17), this correction can be expressed in general algebraic form by:

$$F_s = \frac{F_{t_1} - (t_1/t_2)\, F_{t_2}}{1 - t_1/t_2} \qquad [81]$$

in which:

F_s = Shear force over plate area

F_{t_1} = Total force on plate of first thickness

F_{t_2} = Total force on plate of second thickness

t_1 = Thickness of first plate

t_2 = Thickness of second plate

TABLE II Inertial Correction Factors

Plate	* T_o sec	* T sec	** p $\frac{lb.}{in.}$	** m slugs	* n $\frac{lb.sec}{rt}$	Wave 1	2	3	4	5	6	7	8	9	Factor
1/8"	.215	.204	6.76	.086	.091	.98	.98	.99	.99	.97	.96	.94	.94	.96	K
						.0056	.0044	.0036	.0026	.0063	.0075	.0087	.0089	.0068	Ψ rad.
1/4"	.276	.290	6.76	.173	.183	.95	.97	.98	.99	.94	.91	.89	.88	.93	K
						.0115	.0090	.0073	.0052	.0132	.0158	.0186	.0192	.0142	Ψ rad.

* Measured, ** Calculated

Since the plate area was 1 sq.ft. these shear force values are identical in magnitude to the desired values of shear stress.

A summary of the final shear stress values is presented in Table III for all nine test waves.

A summary of the raw, uncorrected data is presented in Appendix A.

The time variation of τ_o is illustrated in the sample data plot, Fig. [8].

VI PRESENTATION AND DISCUSSION OF RESULTS

A. Average Resistance Coefficients

Comparison of the measured average shear stresses as listed in Table III with the theoretical values was accomplished through use of the average resistance coefficients, C_f, defined in Section III.

Experimental values of the mean coefficient were calculated using Eq. [50] and compared, at average Reynolds numbers given by Eq. [51], with the three theoretical models considered initially.

The results of this comparison are given in Fig. [9]. The conventional unseparated shear wave solution (Eq. [54]) can be seen to yield coefficients and thus average shear stresses much smaller than actually observed.

The bottom velocity gradients of the Karman-Polhausen velocity distribution are so small that even with boundary layer reformation the coefficients (Eq. [57]) are smaller than for the unseparated shear wave.

Measurements of the net (mass transport) velocity distribution (see Ref. 19) indicate that the maximum boundary layer thickness is closely given by Eq. [43] and furthermore that the velocity gradients near the wall are much greater than predicted for unseparated flow. The shear wave velocity distribution was thus used within the reforming boundary layer by letting the length of the shear wave equal the local boundary layer thickness.

Average resistance coefficients computed in this fashion (Eq. [60]) can be seen to agree well with the experiments except at low Reynolds numbers.

The reason for this low Reynolds number divergence between theory and experiment is not clear. Since the magnitude of R varies directly with the wave period, however, it is believed that this disagreement results from some unaccounted for dynamic behavior of the force balance.

Of particular importance is the realization, from Fig. [9] that the experimental resistance coefficients do vary with $R^{-1/2}$ and therefore, for the waves tested, flow in the boundary layer was laminar. The value of R at which transition to turbulent motion will occur has not been determined.

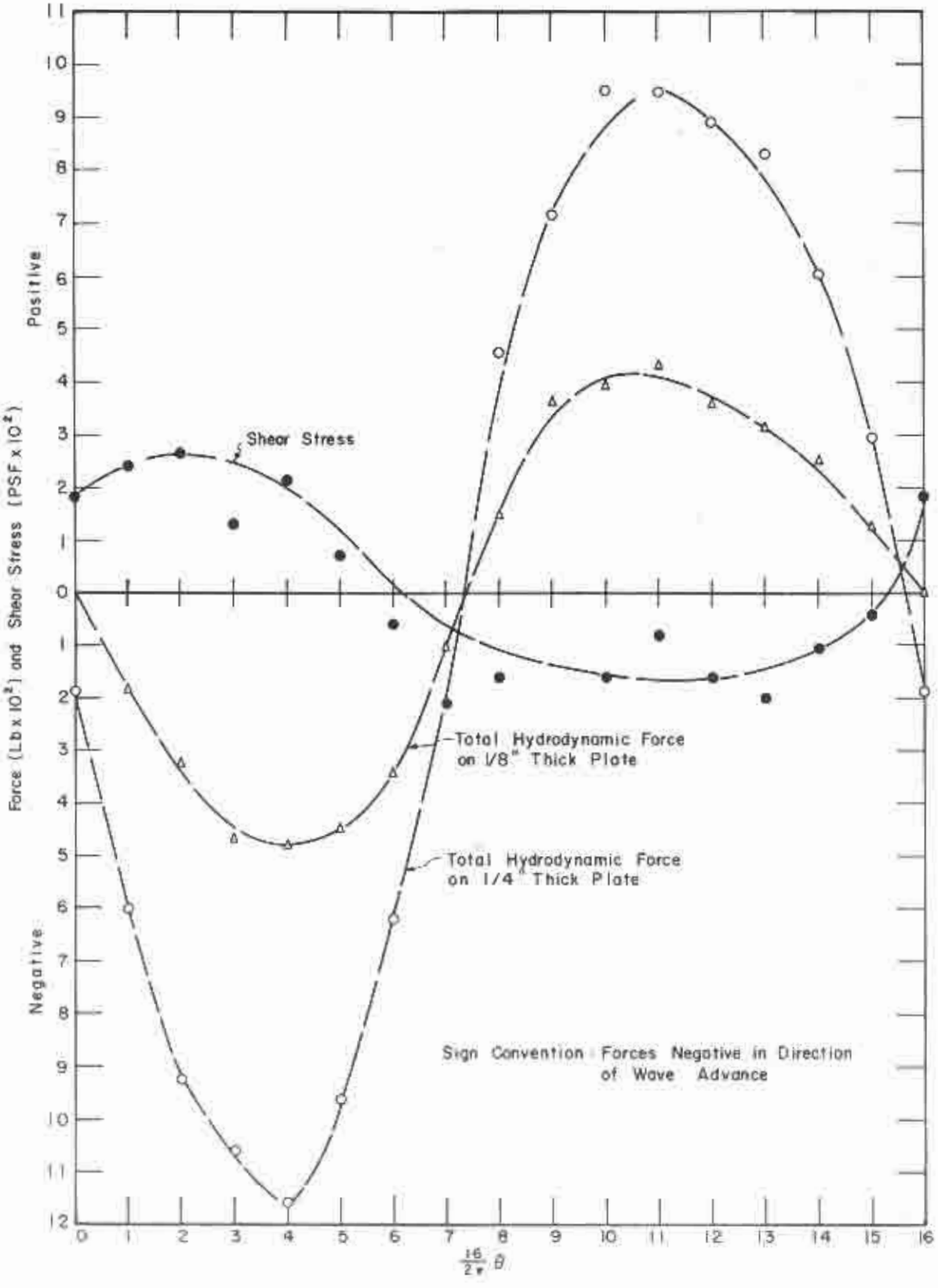

Fig. 8 Sample Time Variation of Measured Forces, Wave No. 3

TABLE III Summary of Measured Bottom Shear Stresses

Wave → / Phase ↓	1	2	3	4	5	6	7	8	9
θ^{o*}	Values of τ_o in lb. per ft^2 x 10^2								
0	-2.18	0.20	1.86	1.19	-0.65	1.27	-1.32	4.11	0.93
22.5	-2.69	-1.00	2.42	0.20	0.28	0.48	3.75	0.85	2.26
45	-0.66	-1.43	2.67	1.17	-0.59	1.40	1.56	3.37	1.92
67.5	-1.12	-0.87	1.29	0	-1.21	0.10	1.06	1.78	1.30
90	-2.86	-0.10	2.18	-1.78	-1.43	-0.62	0.99	0.99	0.65
112.5	-0.86	-0.09	0.71	-1.69	-1.35	-0.16	1.35	-0.97	0.17
135	-0.22	1.10	-0.61	-0.29	-0.02	-0.39	0.92	-2.40	0.03
157.5	-1.70	3.19	0.08	-0.10	0.66	-0.42	-0.55	-2.56	0.42
180	0	1.79	-1.60	-0.99	0.37	-0.57	-0.94	-2.18	-0.93
202.5	0.53	2.39	-0.18	-1.48	1.20	-1.20	-1.20	-1.73	-1.72
225	2.98	1.07	-1.59	1.79	1.73	-1.48	-1.19	-2.67	-0.87
247.5	-1.05	1.48	-0.79	4.40	-0.11	-0.74	-1.65	-3.29	-0.92
270	4.55	-1.36	-1.60	2.22	0.13	-1.00	-1.12	-1.99	-1.10
292.5	1.06	-0.90	-1.99	2.69	0.60	-1.36	-0.50	0.92	-1.02
315	-1.46	-1.71	-1.02	1.99	-0.52	-0.04	-0.18	3.32	-0.12
337.5	1.36	-1.34	-0.36	1.30	-1.59	1.51	0.89	2.32	-0.51
$\lvert\overline{\tau_o}\rvert$	1.58	1.26	1.31	1.45	0.78	0.80	1.20	2.22	0.93
R^{**}	$7.54\text{x}10^3$	$7.54\text{x}10^3$	$2.05\text{x}10^4$	$2.70\text{x}10^4$	$3.77\text{x}10^3$	$1.12\text{x}10^3$	$4.29\text{x}10^2$	$2.73\text{x}10^2$	$1.38\text{x}10^3$

$^*U = \frac{f}{q} \sin\theta$, $^{**}R = \frac{\pi}{2} \frac{f^2}{\nu\theta^3}$

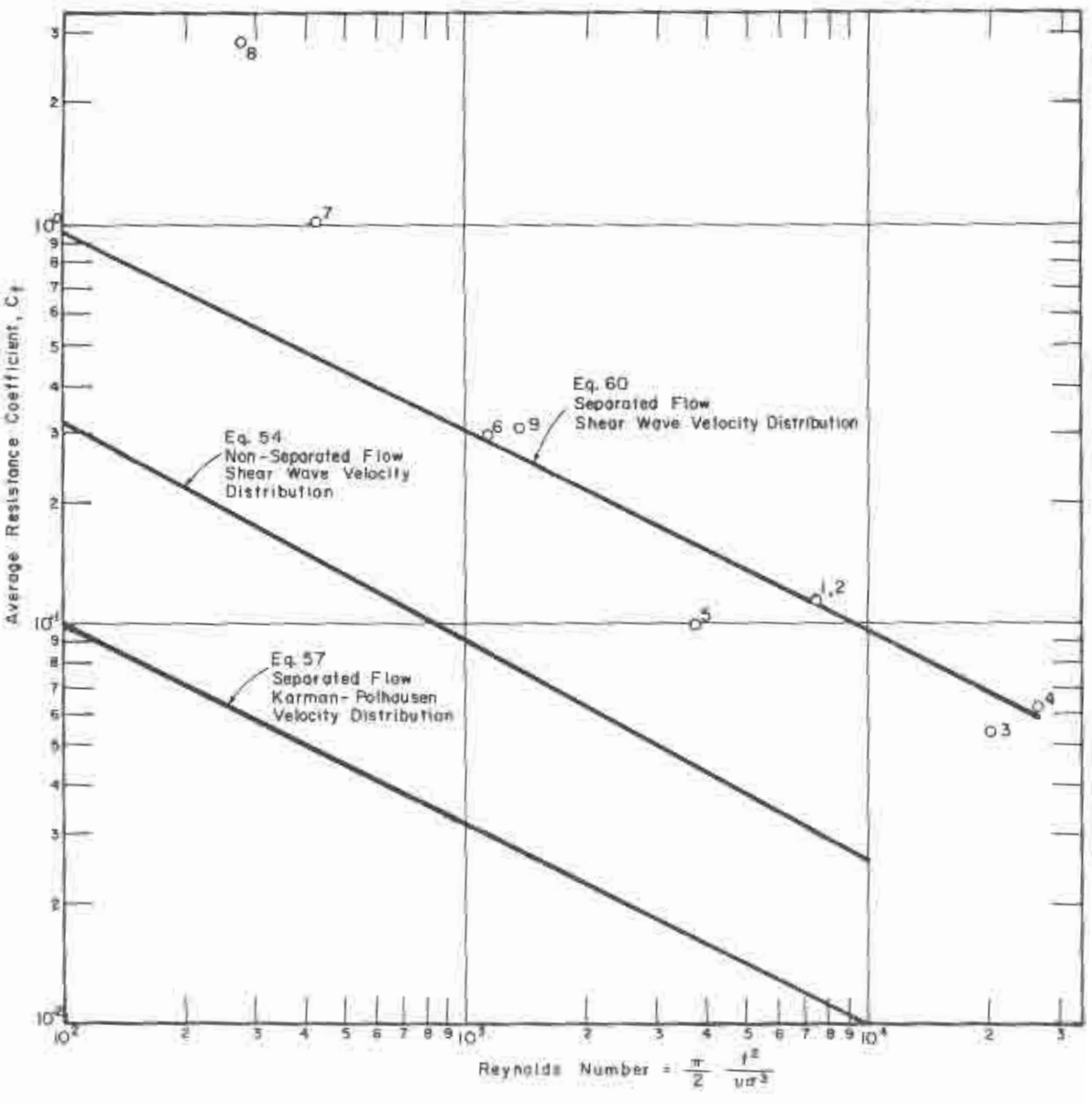

Fig. 9 Average Resistance Coefficients

B. Instantaneous Shear Stresses

Because of the difficulty of defining a local resistance coefficient which does not vary between zero and infinity during each wave cycle the instantaneous behavior was compared with theory through the distribution of local shear stress with wave phase.

This is done dimensionlessly in Fig. [10]. It is here that the difficulties with the experimental technique become apparent. Determination of a small shearing stress by subtracting two much larger quantities produces a wide scatter of individual measurements although as was seen above the mean values over a given wave agree quite well with theory. It should be noted that because of the scale chosen values for wave No. 8 could not be displayed.

As further support to the use of the shear wave velocity distribution the phase angles Θ' and Θ'' of zero bottom shear stress (assumed separation points) were interpolated and compared with those obtained from Eq. [44] and its complement for the other half cycle. This comparison is presented in Table IV and once again, while individual values scatter, the average for all nine waves is within 8 o/o of the theory and in addition the two experimental averages are exactly π radians apart.

TABLE IV

Phase Angle of Zero Bottom Shear Stress

Theory and Experiment

		Θ' (radians)	Θ'' (radians)
Shear wave theory		2.36	5.50
Experiment Wave No.	1	3.14	6.28
	2	1.80	4.50
	3	2.35	5.95
	4	1.18	3.74
	5	2.35	5.31
	6	1.57	5.50
	7	2.61	5.55
	8	1.77	4.97
	9	2.88	6.02
	Average	2.19	5.32

C. Damping Coefficients

In order to view the dissipative process from the standpoint of decay of wave amplitude Figs. [11] and [12] were prepared.

The measured shear stresses were converted into experimental values of the damping coefficient, ϵ, for the separated and unseparated shear wave solutions

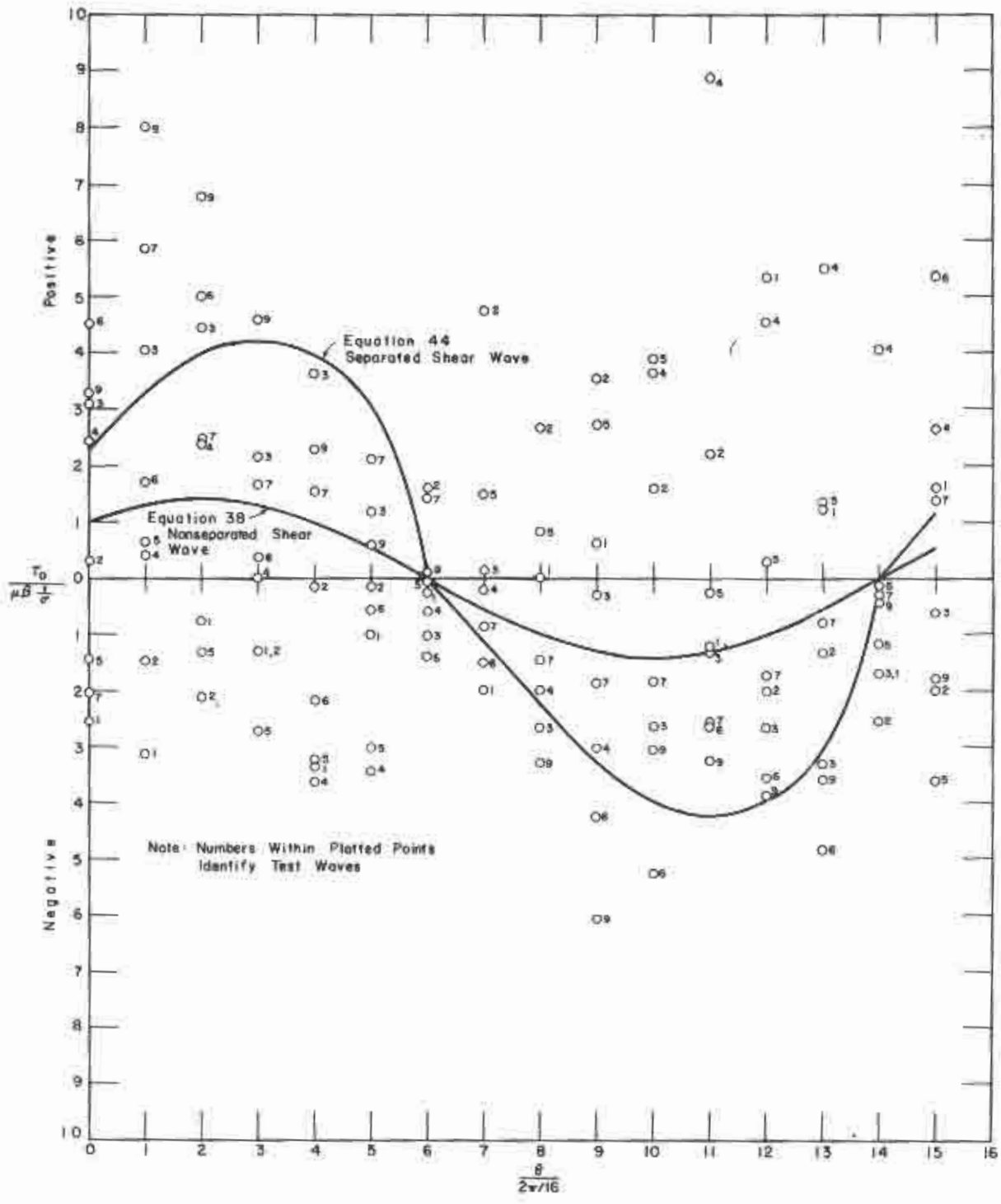

Fig. 10 Time Variation of Instantaneous Shear Stress

by Eqs. [73] and [71] respectively. Theoretical values for the same cases were calculated using Eqs. [74] and [72] respectively.

It should be remembered when examining Fig. [11] that the calculation of the experimental coefficients involves the integral:

$$\int_0^{2\pi} \tau_o \, U \, d\theta \quad \text{and not} \quad \int_0^{2\pi} \left| \tau_o \, U \right| d\theta$$

Consequently the individual coefficients will be very sensitive to phase shift between τ_o and U. This perhaps accounts for the observation that the separated shear wave solution predicts larger damping coefficients than are given by experiment. The data should agree with theory as well here as in the C_f versus R plot of Fig. [9].

In Fig. [12] a further comparison of theoretical and experimental damping coefficients is made, here only for the case of the separated shear wave solution. The relationship between ϵ and d/L is shown for several values of $\beta_o L$ (a Reynolds number) as given by Eq. [74]. Again the experimental values as determined from shear stress measurement and Eq. [73] are displayed and as discussed above differ slightly from the theory for the reasons discussed.

Strong support is given the separated shear wave model by the excellent agreement with this theory offered by damping coefficients determined from amplitude attenuation measurements (Ref. 20). These hitherto unpublished data were generously furnished by the experimenter in the form of amplitude attenuation rates from which the coefficients, ϵ , were calculated by Eq. [61].

VII SUMMARY AND CONCLUSIONS

Analytical and experimental determinations were made of the shear stress exerted on smooth bottoms by oscillatory waves.

The analytical study involved the major assumptions of; (1) a periodic boundary layer separation and regrowth; (2) a laminar, shear wave, velocity distribution within the boundary layer; (3) the length of the shear wave being equal to the local boundary layer thickness.

The experimental study was accomplished by direct measurement of the forces exerted on a test plate inserted in a false bottom. Experiment and theory were compared; (1) through the use of average (over one wave length) shear stresses to define average resistance coefficients in terms of a wave Reynolds number and; (2) through use of instantaneous rates of energy dissipation to define amplitude attenuation coefficients in terms of wave properties and a Reynolds number. The latter comparison included data of another investigator obtained from amplitude attenuation measurements.

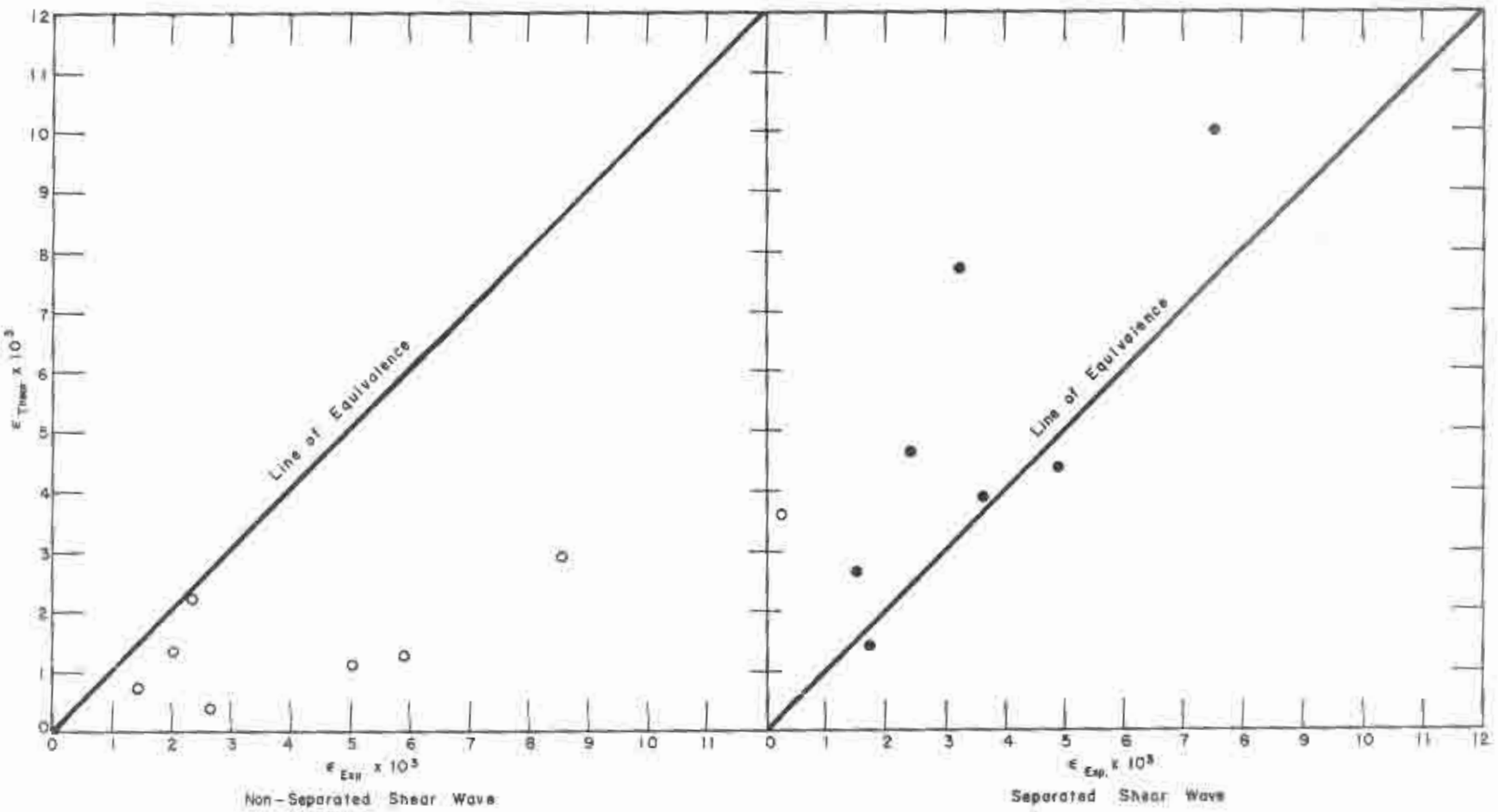

Fig. 11 Comparison of Theories for Damping Coefficients

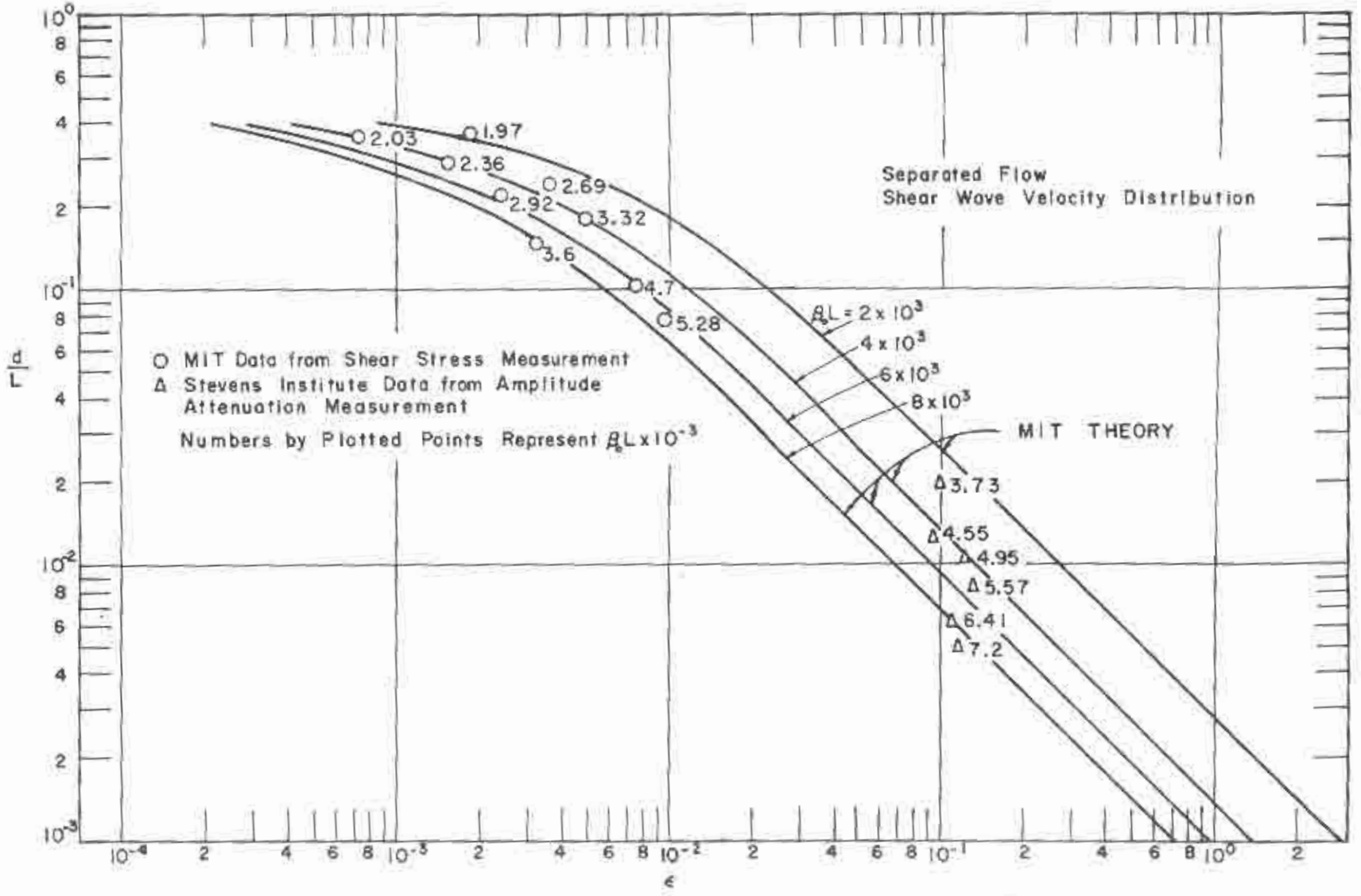

Fig. 12 Damping Coefficients

As a result of these investigations the following conclusions may be drawn:

1. Mean resistance coefficients determined from average (over one wave) bottom shearing stresses vary with $R^{-1/2}$ indicating laminar boundary layers under oscillatory waves at least up to a $R = \frac{\pi}{2}\frac{f^2}{\nu\sigma^3}$ of 3×10^4.

2. Bottom shear stresses measured under oscillatory waves are many times larger than those predicted by the so-called "shear wave" solution of the linearized Navier-Stokes equations.

3. Average resistance coefficients and damping (amplitude attenuation) coefficients may be accurately predicted for laminar motion using a theory based on the assumption of a periodically separating and reforming boundary layer. These coefficients are respectively:

$$C_f = 9.75\, R^{-1/2}$$

in which $$R = \frac{\pi}{2}\frac{f^2}{\nu\sigma^3}$$

and

$$\epsilon = \frac{13.8\,\pi^2}{\beta_o L\,(\sinh 2kd + 2kd)}$$

where

$$\frac{a}{a_o} = e^{-\epsilon\frac{x}{L}}$$

4. The developing laminar boundary layer beneath an oscillatory wave is described by the approximate relationships:

$$\frac{\delta}{[\nu T]^{1/2}} = 1.03\left(\frac{3\pi}{4} - \theta\right)^{1/2}, \quad -\frac{\pi}{4} \le \theta < \frac{3\pi}{4}$$

$$\frac{\delta}{[\nu T]^{1/2}} = 1.03\left(\frac{7\pi}{4} - \theta\right)^{1/2}, \quad \frac{3\pi}{4} \le \theta < \frac{7\pi}{4}$$

in which the origin of θ is 90° behind the wave crest.

ACKNOWLEDGMENT

The generous assistance of Dr. Stephen Lukasik of the Stevens Institute of Technology and the consent of the U. S. Navy in furnishing the data on amplitude attenuation is gratefully acknowledged.

REFERENCES

1. Eagleson, P. S.; Dean R. G. and Peralta, L. A. "The Mechanics of the Motion of Discrete Spherical Bottom Sediment Particles Due to Shoaling Waves," Beach Erosion Board Technical Memorandum No. 104, Washington, 1958.

2. Stokes, G. G., Trans. Cambridge Philosophical Society, Volume IX, 1851, Nos. 20, 21.

3. Boussinesq, J., Journal de Mathematiques Purcs et Appliquees, serie 3e, 4, 335, 1878.

4. Keulegan, G. H. "Gradual Damping of Solitary Waves," Journal of Research, Nat. Bureau of Standards, Res. Paper RP 1895, Vol. 40, Washington, 1948.

5. Bassett, "Hydrodynamics", Cambridge, 1888.

6. Hough, "On the Influence of Viscosity on Waves and Currents," Proc. London Math. Soc., Volume 28, (1), pg. 264, 1896-97.

7. Schlichting, H. "Boundary Layer Theory," McGraw-Hill Book Co., New York, 1955, pg. 67.

8. Biesel, F. "Calcul de l'Amortissement d'une Houle dans un Liquide Visqueux de Profondeur Finie," La Houille Blanche, September-October 1949, pg. 630.

9. Lhermitte, P., "Contribution a l'Etude de la Couche Limite des Houles Monochromatiques," La Houille Blanche, No. Special A, 1958, pg. 366.

10. Lin, C. C., "Motion in the Boundary Layer with a Rapidly Oscillating External Flow," 9th Int. Congress of Applied Mech., Univ. of Brussels, Belgium, September 1956.

11. Nikerson, R. J., "The Effect of Free Stream Oscillations on the Laminar Boundary Layers on a Flat Plate," M.I.T. Dept. of Mechanical Eng. Sc.D Thesis May 1957, (unpublished).

12. Hill, P. G., "Laminar Boundary Layers in Oscillatory Flow," M.I.T. Dept. of Mechanical Eng. Sc.D. Thesis May 1958, also as Report No. 45, Gas Turbine Laboratory, M.I.T. April 1958.

13. Schuh, H., "Calculation of Unsteady Boundary Layer in Two-Dimensional Laminar Flow," Zeitschrift fur Flugwissenschaften, Vol. 1, No. 5, 1953, pg. 122.

14. Lamb, H., "Hydrodynamics," Cambridge University Press, 1932, pg. 622.

15. Ippen, A. T. and Eagleson, P. S. "A Study of Sediment Sorting by Waves Shoaling on a Plane Beach," Beach Erosion Board Technical Memorandum No. 63, Washington, 1955.

16. Harleman, D. R. F. and Shapiro, W. C., "Experimental and Analytical Studies of Wave Forces on Basic Components of Offshore Structures, Part I: Results for Vertical Cylinders," M.I.T. Hydrodynamics Laboratory, Technical Report No. 19, May 1955.

17. Ippen, A. T. and Mitchell, M. M. "The Damping of the Solitary Wave from Boundary Shear Measurements," M.I.T. Hydrodynamics Laboratory, Technical Report No. 23, 1957.

18. Den Hartog, J. P., "Mechanical Vibrations," McGraw-Hill Book Co., Inc. New York, 1947.

19. Eagleson, P. S. and Dean R. G. "Wave-Induced Motion of Discrete Bottom Sediment Particles," Proceedings A.S.C.E. (to be published).

20. Lukasik, S. and Grosch, C., unpublished experiments made at the Experimental Towing Tank, Stevens Institute of Technology, Hoboken, N. J., June, 1958.

APPENDIX A

Summary of Raw Data

I. Measured Forces on Thick Plate, lb. x 10^2

Wave → / Phase ↓	1	2	3	4	5	6	7	8	9
θ, DEG.									
0	- 0.8	- 0.6	- 1.9	- 1.2	0.7	- 1.4	2.0	- 0.6	- 1.0
22.5	- 5.0	- 2.8	- 6.1	- 2.1	- 3.6	- 5.6	- 2.1	- 3.1	- 4.7
45	- 8.8	- 5.0	- 9.4	- 4.8	- 6.4	- 8.7	- 5.15	- 6.6	- 6.6
67.5	-11.1	- 8.4	-10.8	- 6.0	- 8.0	- 9.4	- 7.75	- 8.0	- 7.8
90	-11.0	-10.0	-11.9	- 6.4	- 9.2	- 8.7	- 8.3	- 6.9	- 7.5
112.5	- 9.6	- 9.0	- 9.8	- 7.1	- 9.4	- 7.2	- 6.8	- 3.4	- 7.0
135	- 7.6	- 7.4	- 6.25	- 7.3	- 7.2	- 4.65	- 4.0	- 1.0	- 5.4
157.5	- 4.4	- 5.0	- 2.1	- 6.5	- 4.0	- 1.65	- 1.5	- 0.5	- 2.3
180	0	0.59	4.65	- 2.6	- 0.8	2.1	0	0.55	1.0
202.5	4.6	4.4	7.3	4.3	2.4	4.9	2.2	2.4	3.7
225	8.0	8.4	9.7	7.4	6.0	6.9	4.3	5.6	5.9
247.5	10.4	10.0	9.7	7.15	9.4	8.5	6.5	7.8	7.8
270	11.1	10.8	9.1	7.75	10.6	8.7	7.6	7.4	8.0
292.5	9.8	8.6	8.5	6.8	10.1	7.6	6.7	4.3	7.5
315	7.3	5.8	6.2	3.5	8.6	5.95	4.65	2.0	6.1
337.5	3.3	3.4	3.0	1.6	5.4	3.2	2.80	1.2	2.8

II. Measured Forces on Thin Plate, lb. x 10^8

Wave → / Phase ↓	1	2	3	4	5	6	7	8	9
Θ, Deg.									
0	-1.5	-0.2	0	0	0	0	1.65	1.9	0
22.5	-3.8	-1.9	-1.8	-0.95	-1.6	-2.3	1.0	-1.0	-1.1
45	-4.6	-3.2	-3.3	-1.8	-3.4	-3.4	-1.6	-1.3	-2.2
67.5	-6.0	-4.6	-4.7	-3.0	-4.5	-4.4	-3.1	-2.8	-3.1
90	-6.8	-5.0	-4.8	-4.1	-5.2	-4.45	-3.4	-2.7	-3.3
112.5	-5.1	-4.5	-4.5	-4.4	-5.25	-3.5	-2.5	-2.1	-3.3
135	-3.8	-3.1	-3.4	-3.8	-3.5	-2.4	-1.4	-1.75	-2.6
157.5	-3.0	-0.85	-1.0	-3.3	-1.6	-1.0	-1.0	-1.6	-0.9
180	0	1.2	1.5	-1.8	-0.2	0.7	-0.5	-0.9	0
202.5	2.5	3.4	3.7	1.4	1.8	1.7	0.4	0.2	0.90
225	5.4	4.7	4.0	4.6	3.8	2.5	1.4	1.2	2.4
247.5	4.5	5.6	4.4	5.8	4.5	3.65	2.2	1.9	3.3
270	7.7	4.6	3.7	5.0	5.2	3.6	3.0	2.4	3.3
292.5	5.3	3.8	3.2	4.25	5.2	2.9	2.9	2.5	3.1
315	2.8	2.0	2.55	2.75	3.9	2.8	2.1	2.7	2.9
337.5	2.3	1.0	1.3	1.45	1.8	2.3	1.8	1.8	1.1

BEACH EROSION BOARD, C.E., U.S. ARMY, WASH., D.C.

THE DAMPING OF OSCILLATORY WAVES BY LAMINAR BOUNDARY LAYERS by P. S. Eagleson, Aug. 1959, 38 pp., 4 tables, 12 illus., and appendix. TECHNICAL MEMORANDUM NO. 117 UNCLASSIFIED

1. Wave forces - Bottom stress
2. Shear stresses - Wave-bottom
I. Eagleson, P. S.
II. Title

Results of an analytical and experimental investigation of the shearing stresses exerted on a smooth bottom by passage of oscillatory water waves are presented. Force measurements including time-history of instantaneous force during passage of waves and simultaneous measurements of instantaneous wave characteristics were made and corrected for pressure and inertia forces to obtain net tangential forces. Average resistance and damping coefficients were derived in terms of wave properties. Analysis of experimental results using these coefficients consistently showed experimental bottom shearing stresses greatly exceedhd those predicted by theory. The boundary layer was then assumed to be disrupted each half cycle due to flow separation, and periodic regrowth of the layer was calculated by the approximate momentum technique. Resistance and damping coefficients calculated on this basis show generally excellent agreement with experiment.

BEACH EROSION BOARD, C.E., U.S. ARMY, WASH., D.C.

THE DAMPING OF OSCILLATORY WAVES BY LAMINAR BOUNDARY LAYERS by P. S. Eagleson, Aug. 1959, 38 pp., 4 tables, 12 illus., and appendix. TECHNICAL MEMORANDUM NO. 117. UNCLASSIFIED

1. Wave forces - Bottom stress
2. Shear stresses - Wave-bottom
I. Eagleson, P. S.
II. Title

Results of an analytical and experimental investigation of the shearing stresses exerted on a smooth bottom by passage of oscillatory water waves are presented. Force measurements including time-history of instantaneous force during passage of waves and simultaneous measurements of instantaneous wave characteristics were made and corrected for pressure and inertia forces to obtain net tangential forces. Average resistance and damping coefficients were derived in terms of wave properties. Analysis of experimental results using these coefficients consistently showed experimental bottom shearing stresses greatly exceeded those predicted by theory. The boundary layer was then assumed to be disrupted each half cycle due to flow separation, and periodic regrowth of the layer was calculated by the approximate momentum technique. Resistance and damping coefficients calculated on this basis show generally excellent agreement with experiment.

BEACH EROSION BOARD, C. E., U.S. ARMY, WASH., D. C.

THE DAMPING OF OSCILLATORY WAVES BY LAMINAR BOUNDARY LAYERS by P. S. Eagleson, Aug. 1959, 38 pp., 4 tables, 12 illus., and appendix. TECHNICAL MEMORANDUM NO. 117 UNCLASSIFIED

1. Wave forces - Bottom stress
2. Shear stresses - Wave-bottom
I. Eagleson, P. S.
II. Title

Results of an analytical and experimental investigation of the shearing stresses exerted on a smooth bottom by passage of oscillatory water waves are presented. Force measurements including time-history of instantaneous force during passage of waves and simultaneous measurements of instantaneous wave characteristics were made and corrected for pressure and inertia forces to obtain net tangential forces. Average resistance and damping coefficients were derived in terms of wave properties. Analysis of experimental results using these coefficients consistently showed experimental bottom shearing stresses greatly exceeded those predicted by theory. The boundary layer was then assumed to be disrupted each half cycle due to flow separation, and periodic regrowth of the layer was calculated by the approximate momentum technique. Resistance and damping coefficients calculated on this basis show generally excellent agreement with experiment.

BEACH EROSION BOARD, C.E., U.S. ARMY, WASH., D. C.

THE DAMPING OF OSCILLATORY WAVES BY LAMINAR BOUNDARY LAYERS by P. S. Eagleson, Aug. 1959, 38 pp., 4 tables, 12 illus., and appendix. TECHNICAL MEMORANDUM NO. 117. UNCLASSIFIED

1. Wave forces - Bottom stress
2. Shear stresses - Wave-bottom
I. Eagleson, P. S.
II. Title

Results of an analytical and experimental investigation of the shearing stresses exerted on a smooth bottom by passage of oscillatory water waves are presented. Force measurements including time-history of instantaneous force during passage of waves and simultaneous measurements of instantaneous wave characteristics were made and corrected for pressure and inertia forces to obtain net tangential forces. Average resistance and damping coefficients were derived in terms of wave properties. Analysis of experimental results using these coefficients consistently showed experimental bottom shearing stresses greatly exceeded those predicted by theory. The boundary layer was then assumed to be disrupted each half cycle due to flow separation, and periodic regrowth of the layer was calculated by the approximate momentum technique. Resistance and damping coefficients calculated on this basis show generally excellent agreement with experiment.